1. Analysis of Deposits Formed During Biomass Co-firing on 15Mo3 Under Different Gas and Temperature Conditions

V.F.Lay[1*], R.L.Higginson[1], S.C.Hogg[1], C.A.Kirk[2], C.Davis[3]

1. Department of Materials, Loughborough University, Loughborough, Leicestershire, LE11 3TU

2. Department of Chemistry, Loughborough University, Loughborough, Leicestershire, LE11 3TU

3. E.On New Build & Technology Limited, Technology Centre, Ratcliffe-On-Soar, Nottingham, NG11 0EE

2. Abstract

This paper reports on the analysis of fly ash and oxides on 15Mo3 after the co-firing of eucalyptus and a Russian coal at various temperatures and gas conditions for 50 hours. The loose deposits present have been characterised using X-Ray Diffraction (XRD), Scanning Electron Microscopy (SEM) and Energy Dispersive X-Ray Spectroscopy (EDS). Results show that under reducing conditions KCl deposition is increased and a variation in oxide scale composition is observed. Complex silicates, often present as spheres are imaged through SEM.

3. Keywords

Low-Alloy Steel, 15Mo3, Co-Firing, Oxidation.

4. Introduction

Low-alloy steels such as 15Mo3 are often used as structural materials in power plants due to their lower cost compared to other ferritic and heat-resistant steels[1,2,3]. 15Mo3 is typically used for boiler tubes for plants operating at temperatures up to 475°C. Oxidation can lead to serious problems including pipe failure and wall thinning at higher temperatures[4]. A review of high temperature oxidation of low alloy steels has previously been conducted by Chang and Wei[5], and further research characterising the oxides formed from low alloy steels has been conducted by Higginson *et al.*[6] where it was concluded that low alloy steels tend to form less complex oxides such as wustite, magnetite and hematite. Later work by Chang[4] also showed that long-term oxidation of metals could not be predicted as different alloys possess widely differing spalling characteristics.

The co-firing of biomass and coal is an increasingly popular method to reduce CO_2 emissions from energy generation[7]. Biomass unlike coal is considered to be carbon neutral. Power stations typically used for the combustion of coal are being adapted to also fire biomass. Ash composition from biomass can vary widely and deposits often form in different regions compared to 100% coal-fired systems[8]. These deposits affect heat transfer and can often lead to premature boiler tube failure[9]. Information on oxidation products and deposit formation on 15Mo3 during the combustion of biomass is essential to minimise plant down

time. The change from firing coal to co-firing presents challenges for materials due to the chemical differences between coal and biomass.

Biomass commonly has a higher chlorine and potassium content compared to coal, which can lead to increased corrosion compared to coal firing alone[10]. Silicates and their role in combustion have been widely investigated by Vassilev *et al.*[11]in which it was suggested that they prevent the formation of harmful KCl by means of potassium capture. Frandsen[12] found that the uptake of potassium through silicates prevented the formation of corrosive KCl. K_2SO_4 is present in the samples analysed by Frandsen and so, the harmful KCl may have been sulphated through the mechanism proposed by Kassman *et al.*[13] in **Equation 1**.

$$2KCl + SO_2 + H_2O + {}^1/_2\, O_2 \rightarrow K_2SO_4 + 2HCl \qquad (1)$$

Along with the capture of potassium to form alkali silicates other metals often react with the SiO_2 inherent in both the biomass and coal. Complex silicates such as feldspars form during combustion either through agglomeration of ash particles in the flue gas or via chemical reaction in the deposit itself[8].

A Cl containing atmosphere either through the presence of deposited KCl or HCl(g) can lead to active oxidation; a schematic illustration can be seen in **Figure 1**. Under reducing conditions an oxide barrier which is defective and far less protective than an oxide layer formed under conditions of high O_2 is likely due to little O_2 present to react and form a protective layer [14]. A presence of CO at concentrations higher than 2% has previously been shown to increase the corrosive rate of HCl by 2.5 times[15]. A high $\%O_2$ indicates oxidising conditions, under which protective oxide scales are more likely to form[14]. In the high $p(O_2)$ metal chlorides diffuse to the scale surface and upon encountering a higher $p(O_2)$ gradient solid metal oxides are formed in a loosely adherent non-protective, porous layer[15].

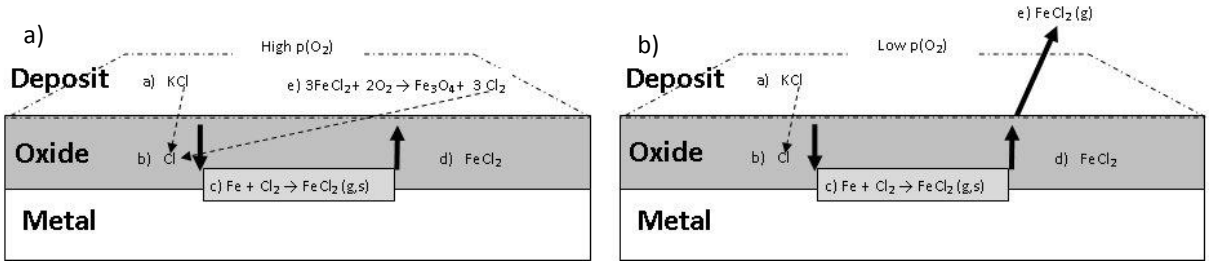

Figure 1: Active oxidation mechanisms under a) oxidising and b) reducing conditions adapted from reference 12

Deposit formation and ash phases are widely researched topics within the field of co-firing. Vassilev *et al*.[11] conducted an extensive review into the phases found in fly ash and deposits, their roles in corrosion and in relation to their environmental concerns. Fly ash interactions and deposition mechanisms have been discussed in great detail in 'The Handbook of Biomass Combustion and Co-firing'[8] which gives information about inorganic phase interactions. This allows insight into possible deposition mechanisms to be gathered as information on both coarse fly ash particles and aerosols are given. Zbogar *et al*.[9] discuss the six methods of particle deposition related to deposit growth:

- Inertial Impaction
- Thermophoresis and Diffusion
- Eddy Deposition (Flue Gas flow side)
- Eddy Deposition (Non Flue-Gas flow side)
- Chemical Reaction
- Condensation

Eucalyptus is a low ash, low chlorine fuel which decreases the likelihood of large harmful deposits[16]. Knowledge of the interaction between coal and biomass when co-fired can lead to insights into the corrosive effects along with possible areas of deposition. An investigation of the corrosive effect of a eucalyptus/coal blend on 15Mo3 at varying temperatures under oxidation/reducing conditions is reported in this paper.

5. Materials and Experimental Procedure

The composition of the alloy 15Mo3 is shown in Table 1. Probes containing coupons of the alloy were exposed for 50 hours in a 0.8MWth rig co-firing eucalyptus (82.8 % Thermal) and Russian coal (17.2% Thermal). The fuel was fired in pulverised form at feed rates of 183.50 kg/h (eucalyptus) and 18.89 kg/h (coal). Corrosion coupons of 15Mo3 are a bare metal surface ground to a 0.4RA surface finish. These coupons are flush with the lining of the boiler so as to experience the same gas and temperature conditions as pipes as well as not creating any deviation of gas flow. The probes securing mechanisms were lubricated using Belzona 8211 (H.P. Anti-Seize) mineral based nickel grease. A Eurotherm temperature controller with a continuously variable output was used to drive a proportional air throttle valve, enabling the flow of cooling air to the probe to be regulated. Insertion points of the probes are shown in **Figure 2**.

Samples were taken at various positions on the boiler wall and were subjected to temperatures of 425-450°C under both oxidation and reducing conditions. Sample conditions are shown in Table 2. Probes were removed after 50h exposure and were allowed to cool and the ash debris was removed from the probes for analysis. The ash matrix composition was provided by the E.On New Build and Technology centre, elements

present were determined by acid dissolution and emission spectroscopy according to ASTM D6349-09.

Ash debris was analysed using a LEO 1530VP Field Emission Gun SEM (FEGSEM) with an EDAX Genesis Energy Dispersive X-Ray Spectroscopy (EDS) instrument. Samples were prepared on carbon pads, attached to aluminium stubs followed by coating with gold for 30s. Samples were prepared for X-Ray diffraction (XRD) analysis by placing between two layers of cello tape. Powder XRD data was collected using the Bruker D_8 discover diffractometer (5-65º 2θ, CoKα radiation, 16h). Inductively Coupled Plasma – Optical Emission Spectroscopy (ICP-OES) was conducted by E.On according to the ASTM D6349-09 standard[17].

Table 1: Measured Composition of the Alloy 15Mo3, provided by E.On

Alloy	Cr	Mn	Fe	Ni	Mo	Cu
15Mo3	0.22	0.48	98.59	0.24	0.29	0.18

Table 2: Probe temperatures and atmospheres of samples analysed

Probe	Temperature (°C)	Atmosphere
A	450	Reducing
B	450	Oxidising
C	425	Oxidising

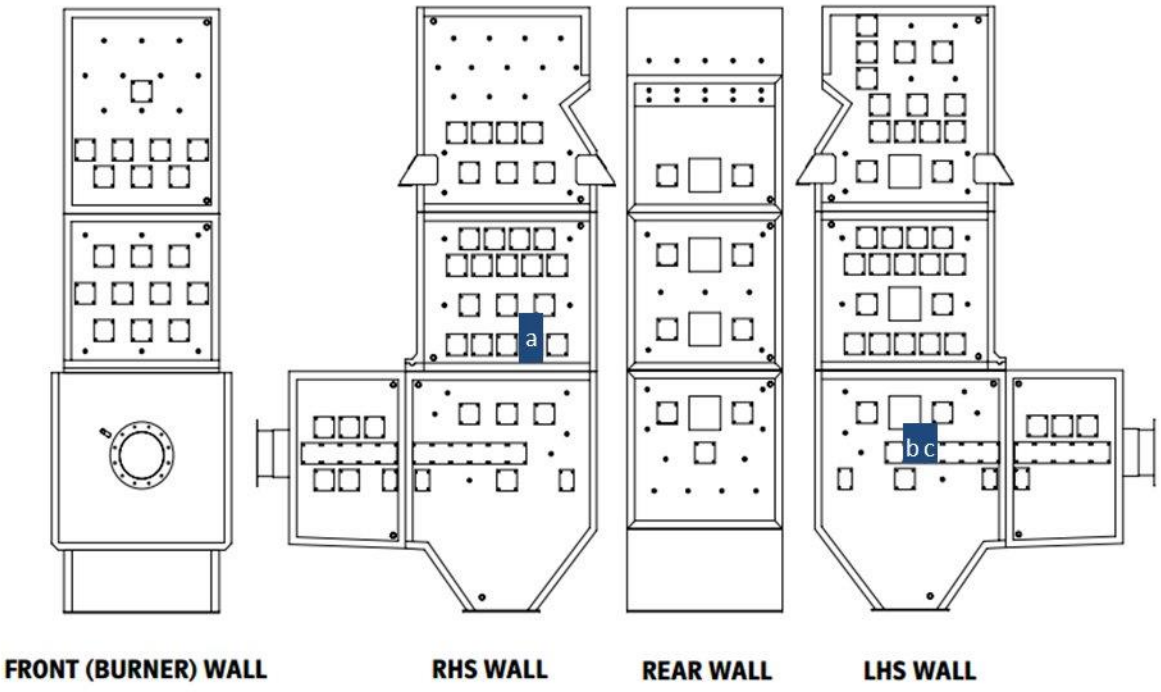

Figure 2: Schematic of the boiler in the combustion rig showing the insertion points of probes a,b and c analysed in this study, provided by E.On

6. Results and discussion

6.1 (a) Fuel Characteristics

Inherent biomass ash, those elements that are present as salts, bound in the carbon structure are often more readily available during combustion than those inorganic salts bound in coal[8]. **Table 3** shows the ash matrix composition of both the biomass and coal blend, elements presented are assumed to be in the oxide form for analysis with ICP-OES, with the exception of Ca, potentially present as $CaCO_3$, due to the aggressive nature of the acid dissolution. A large percentage of the ash matrix is Si, which can also form a large percentage of coal, in the form of complex silicates such as Illite ($(K,H_2O)Al_2(Si,Al)Si_3O_{10}(OH)_2$) and also as less complex silicates like quartz (SiO_2)[12]. Si can also be present in large quantities in biomass giving skeletal system support in some plants[8]. Information on these elements present often gives important insight into phases likely to be present in any deposits formed through the co-firing of eucalyptus and Russian coal.

Table 3: Ash Matrix Composition according to ASTM D6349-09

Phase	Composition Ash Matrix (%)
SiO_2	33.20
Al_2O_3	8.66
Fe_2O_3	5.89
CaO	25.53
MgO	6.41
K_2O	11.06
Na_2O	2.80
TiO_2	0.87
BaO	0.25
Mn_3O_4	1.85
P_2O_5	2.67

6.2 (b) Sample Atmospheres

Figure 3 shows gas profiles of the probes. The gas sampled was dried through a silica gel column prior to analysis the remainder of the atmosphere contains $N_2/CO_2/H_2O$ along with low levels of various sulphur species and NO_x. Clear differences between O_2 and CO concentrations are observed between probes under oxidising and reducing atmospheres; a higher %CO indicates the conditions are reducing. The coupons are exposed at temperatures below 500°C, and therefore it is likely the corrosion will be parabolic[15]. A high $\%O_2$ indicates oxidising conditions, under which protective oxide scales are more likely to form[14]. Samples analysed in the scope of this paper do not show the full oxidation of the metal coupons as only the loose debris removed from the probes was analysed.

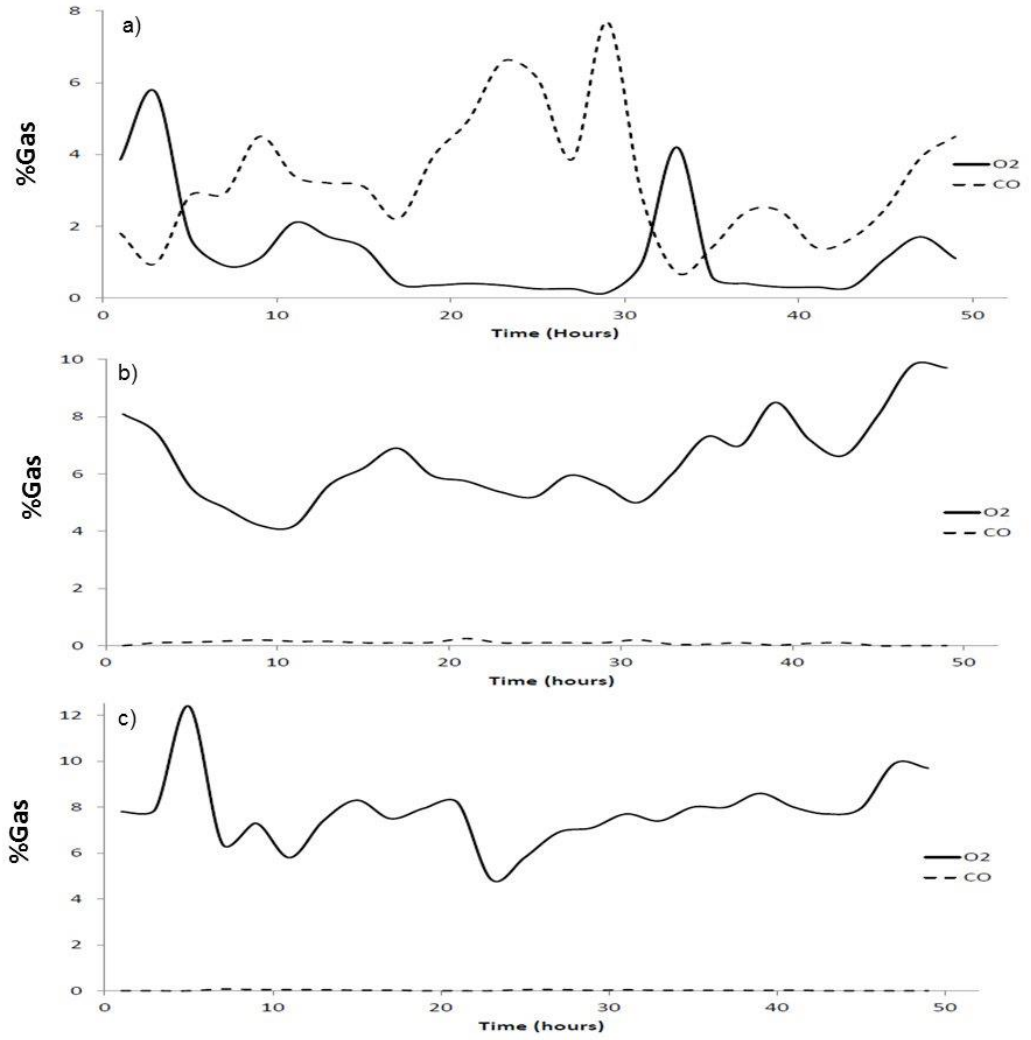

Figure 3: Gas profiles of the three probes during the 50 hour combustion run a) 450°C under a reducing atmosphere b)450°C Under an oxidising atmosphere c) 425°C under an oxidising atmosphere

6.3 (c) XRD Analysis

XRD analysis of the loose deposits from the samples shows the major component in all cases to be quartz (SiO_2). Si constitutes a large percentage of the ash residue and so it is unsurprising that SiO_2 forms a considerable amount of the deposit. During combustion refractory oxides such as SiO_2, CaO and MgO nucleate heterogeneously, the agglomeration of these compounds can lead to the formation of silicates such as sapphirine $(Mg,Al)_8(Al,Si)_6O_{20}$[8] and leucite ($KAlSi_2O_6$). The unassigned peaks in Figure 4 are thought to be due to complex interactions forming solid solutions of silicates. The low intensity of these peaks makes assignment to a specific phase/composition challenging. SEM-EDS analysis confirms the presence of silicate phases in these samples, which provides a strong basis for these tentative assignments (Section (f))

Hematite (Fe_2O_3) and magnetite (Fe_3O_4) are further phases identified in the XRD pattern, suggesting that the polished metal (Fe-alloy) coupons have undergone oxidation. Chang *et al*.[5] in their review of low-alloy metal oxidation at high temperatures state that at below 570°C only magnetite (Fe_3O_4) and hematite (Fe_2O_3) will be present as iron oxides, at higher temperatures wüstite (FeO) will be formed. Previous work by Higginson *et al*.[6] characterising the phases in low-alloy steels at high temperature, was consistent with these findings. Cr_2O_3 was also found to be present, even though the Cr content of the alloy is low. Reasons for this apparent enrichment will be discussed in section (d).

In this study, KCl was found to be present in the sample collected under reducing conditions (Figure 4**, S**). Pettersson *et al*.[18] showed that KCl deposits on the surface of a 304-type austenitic alloy lead to an increase in breakaway oxidation, particularly around grain boundaries. As greater amounts of KCl are present in the reducing atmosphere it is likely more breakaway oxidation has occurred and therefore upon cooling the scales have become loose. This could also explain the greater variation in composition of the oxides in the scales formed under the reducing atmosphere.

The Ni present as both NiO and elemental Ni is likely to come from the anti-seize grease used to allow coupon removal from the probe, rather than an oxidation product of the minimal amount of Ni contained in the alloy.

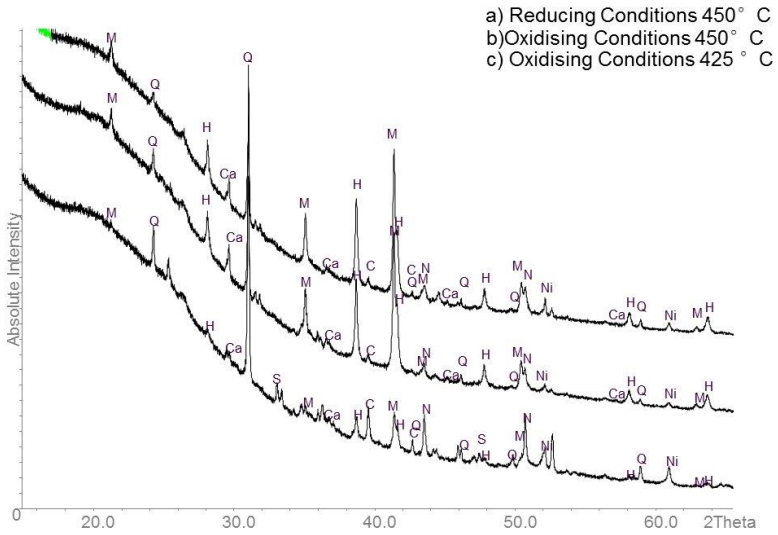

Figure 4: XRD Pattern of Loose Debris Removed from Probes (Key in table 4)

Table 4: XRD phases identified in the samples

Symbol	Phase
M	Magnetite (Fe_3O_4)
Q	Quartz (SiO_2)
H	Hematite (Fe_2O_3)
Ca	$CaSO_4$
S	KCl
C	Cr_2O_3
N	NiO
Ni	Ni (metal)

6.4 (d) Deposit Microscopy

The phases present in the bulk deposit have been determined by XRD (section (c)). EDS analysis of the deposits, imaged using an SEM, are in agreement with the XRD analysis. However some phases are present in quantities too small to be detected using XRD. Figure 5 shows an oxide scale in profile; clear deposit and metal oxide regions can be identified. The probable mechanism of formation of these loose oxide scale fragments is breakaway oxidation followed by loss of the scales upon cooling[19]. These oxide scales have been separated from the alloy during the 50 hour combustion run and are loose enough to be removed by gentle shaking. The fragments of oxide scales show significant variation in size with a range of 35 - 200µm in length and 3-20µm thickness suggesting variation in the oxidation of the metal. This thickness variation could also be due to deposit-oxide interaction.

A linescan of the scale shows K and S to be closely associated in this deposit region. This is likely to be K_2SO_4 deposited homogenously under the diffusion mechanism presented by Zbogar *et al*[9], or KCl that has then reacted with SO_2 according to the reaction given in Equation 1. In comparison, silicate spheres and refractory oxides will deposit through inertial impaction possibly undergoing further complex reactions post-deposition[9].

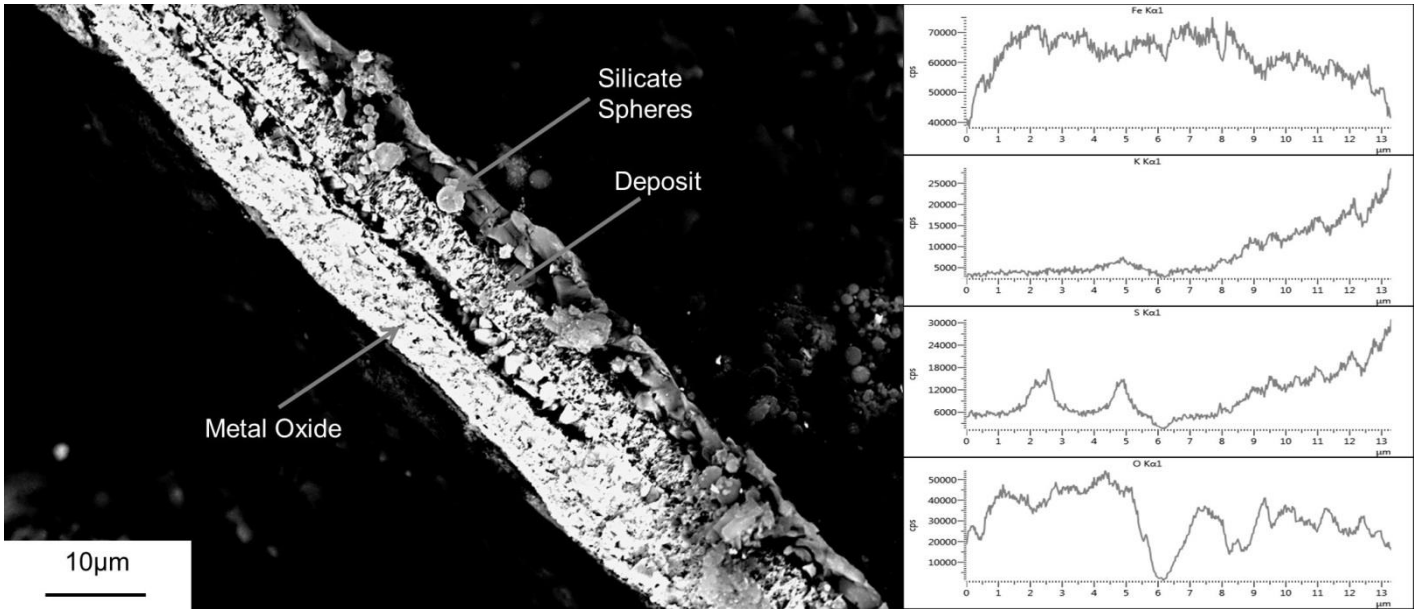

Figure 5: SEM micrograph of an oxide scale formed under oxidising conditions in profile with linescan data

Figure 6 contains an oxide flake with a large amount of KCl deposited on the surface, likely as the result of diffusion. These particles are fairly prominent suggesting a degree of homogeneous nucleation in the flue gas. Large KCl deposits were only imaged on scales found under reducing conditions.

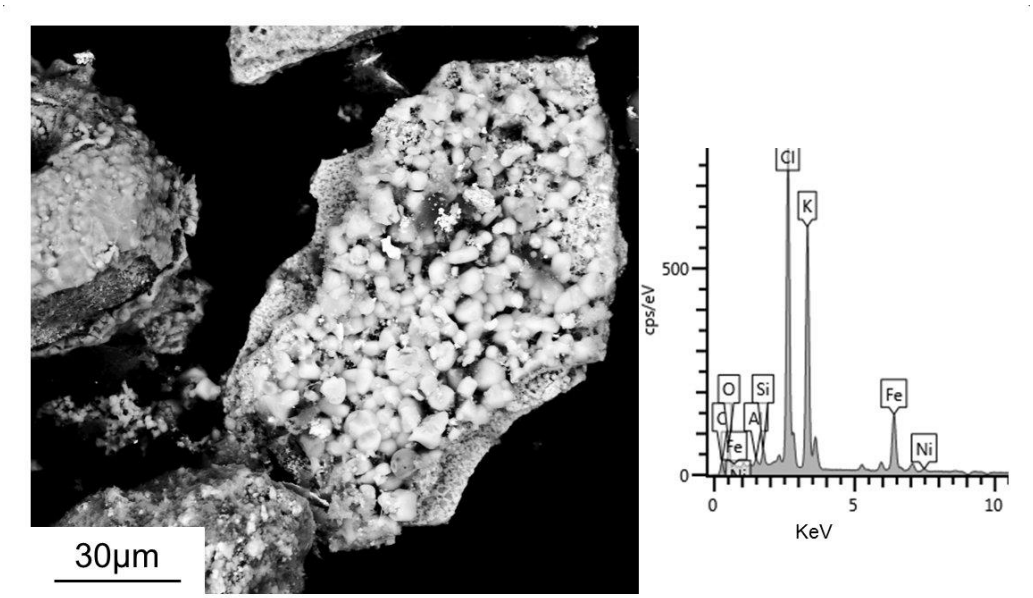

Figure 6: SEM micrograph of KCl deposition onto the surface of an oxide scale under reducing conditions.

In Figure 7 EDS analysis of one of the scales formed in the reducing atmosphere shows the presence of different metal ions, these results fit well with the XRD analysis, showing high amounts of Cr present in the scale, unusual for such a low-alloyed steel. Uusitalo *et al*[20] report Cr enrichment in scales formed under reducing conditions on low-alloy steels; this research supports these findings. Park *et al*[21] also found surface enrichment of Cr under

electrochemically reducing conditions for a low alloy steel with a 0.5%Cr content. Wood[19] stated that the initial Cr oxidation rate in metals with a low Cr content (0.2%) is more rapid in comparison to Fe and that this can lead to a Cr content maximum at the inner/outer scale interface. This oxidation rate is shown to be faster under reducing conditions than oxidising conditions[19]. An increased Cr content of the scale can apparently be explained by this preferential oxidation. Fe and Cr are present in close association with one another, possibly suggesting the presence of an Fe, Cr spinel phase. It should however be noted that the origin of the oxides may be difficult to ascertain in the present case and could be contaminants from the combustion rig, for example.

Potassium and sulphur are once again shown to closely associate with one another (Figure 7) suggesting the presence of K_2SO_4, formed either through diffusion deposition or sulphation of KCl (Equation 1). The presence of Ni throughout the sampled region is likely due to the grease used in the lubrication of the probe.

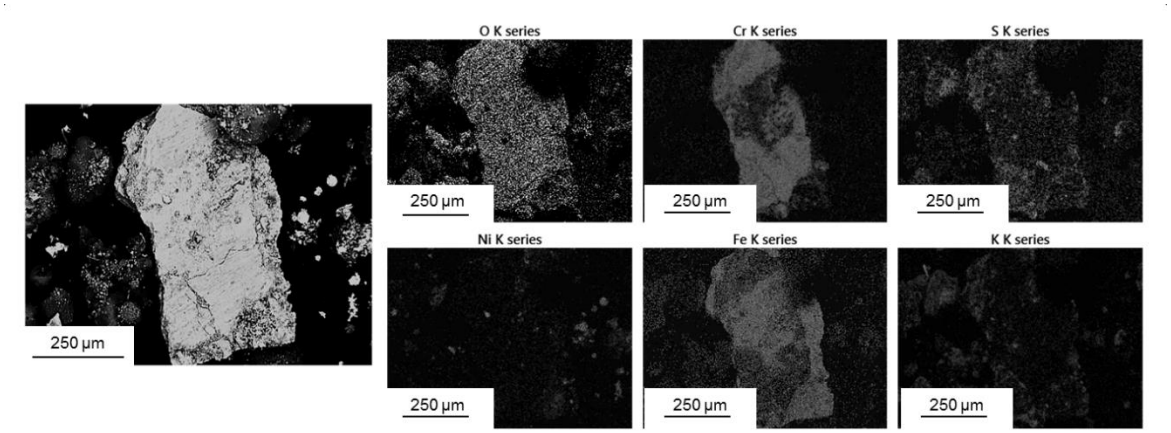

Figure 7: EDS analysis of an oxide scale from reducing conditions at 450°C

6.5 (e) Iron Oxidation Products

6.5.1 Magnetite

Magnetite and hematite are shown to be present from XRD analysis (section (c)), on certain oxide fragments octahedral crystals characteristic of magnetite are present (Figure 8). EDS analyses of these octahedral crystals show that they contain a large amount of Fe and O, alongside minor portions of K, Cl and Ni, confirming the presence of magnetite. The K and Cl, likely to be present as KCl, is thought to have induced $FeCl_2$ transport to the surface of the deposit where upon encountering the O_2 will have formed the octahedral magnetite crystals, through an active oxidation mechanism[14].

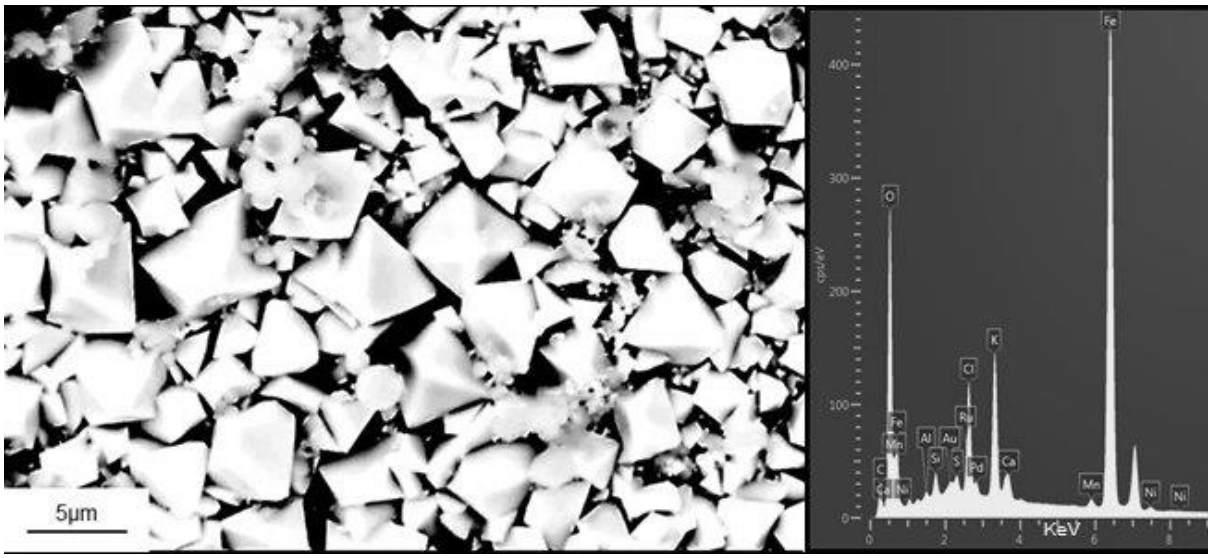

Figure 8: Magnetite Octahedral Crystals visible under both oxidising and reducing conditions, SEM-EDS analysis of the octahedral regions

6.5.2 Hematite

Cracks were often observed in the oxide scale either between the deposit and the oxide or two layers of the oxide itself. At higher magnification (Figure 9) whiskers can be seen growing in these gaps only under oxidising conditions. Previous work by Higginson *et al*.[22] on whisker growth morphology of high temperature oxides showed these whiskers are highly likely to be hematite. Yuan *et al*.[23] found iron whisker growth often occurs on the grain boundaries of hematite/magnetite whereas Higginson *et al*.[22] and Pettersson *et al*.[18] found that whiskers were most likely to form around areas of breakaway oxidation. It is beyond the scope of the current work to speculate on the formation mechanism of the whiskers.

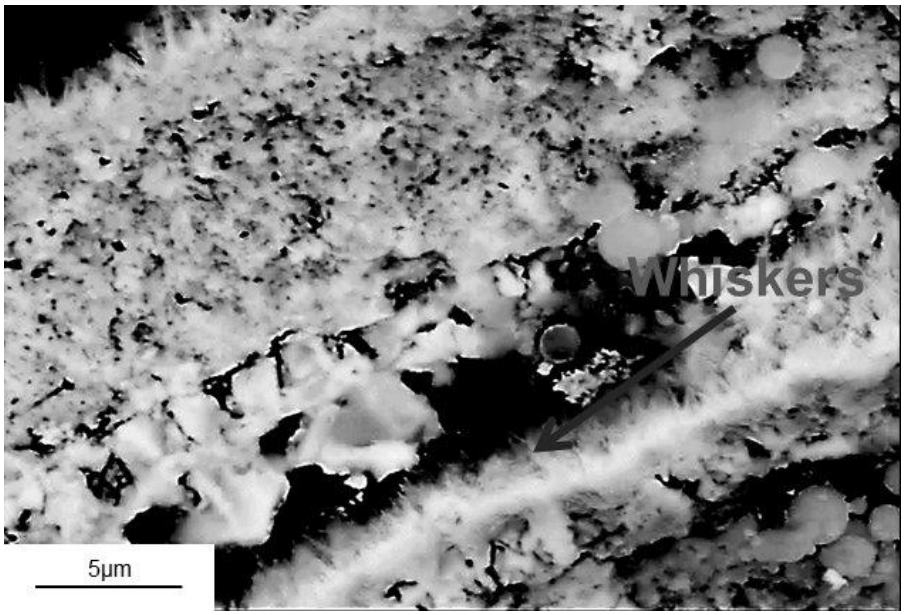

Figure 9: Whiskers, thought to be hematite present under oxidation conditions.

6.6 (f) Spherical Debris

Alongside oxide scales are other non-metallic particles formed as loosely adhering deposits. Amongst this loose fly ash there are multiple particles with different morphologies. Often during biomass combustion, complex silicates form spherical particles either classified as a cenosphere (a microsphere of aluminosilicate glass encapsulating gas[11]) or a plerosphere (a cenosphere encapsulating smaller pre-existing particles[11]).

Figure 10 shows a plerosphere along with cenospheres present in the deposits of all three samples. Raask[24] investigated the formation both cenospheres and plerospheres. Cenosphere formation comes from the expansion of a silicate droplet, often containing a catalytic amount of iron, some carbon must be present in the slag melt in order for gas evolution to occur and so the droplet swells to a hollow sphere. Plerospheres are formed through a similar mechanism however, mineral particles must be deposited through the droplet in order to be encapsulated in the sphere[24]. This spherical debris is thought to have deposited through the inertial impaction mechanism. However, it is thought that as the spheres have not formed large agglomerates, the reactions necessary to form these particles, took place in the flue gas prior to deposition.

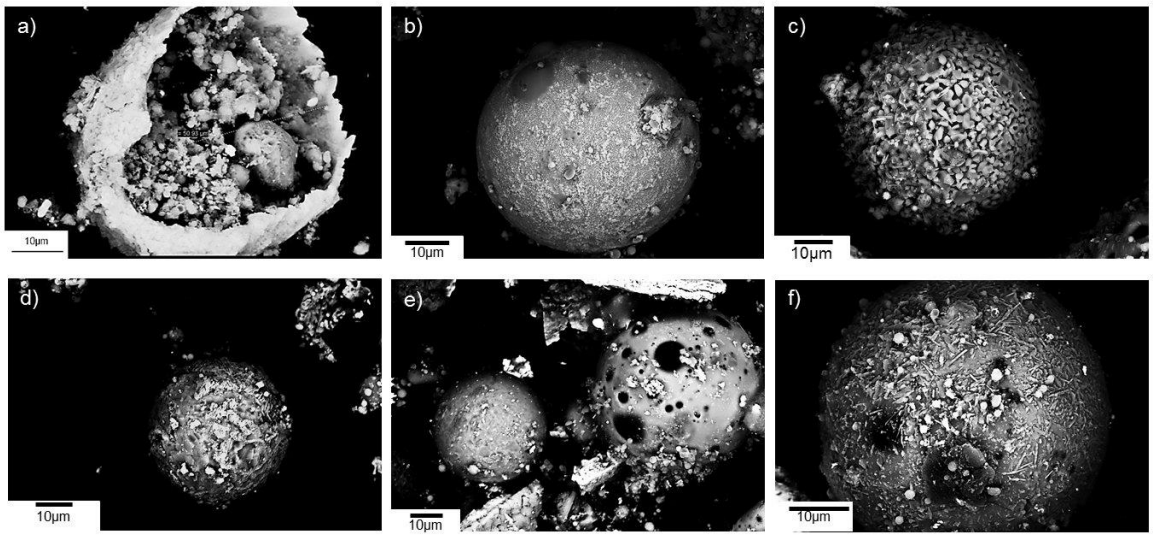

Figure 10: Spherical deposits formed under different conditions (a-c) Oxidising conditions 450°C (d-e) Oxidising Conditions 425°C (f) Reducing Conditions 450°C

Clear differences in the surfaces of the spherical particles can be seen in Figure 10 with some containing large pores (Figure 10e) and others showing signs of surface enrichment (Figure 10c). The composition of the spheres formed can often be highly complex. The spectra from EDS (Figure 11) shows the composition of the two spheres in Figure 10e, illustrating two different compositions of the spherical deposits. Varying amounts of Ca and

K are present in both silicate spheres along with Mg and Na suggesting the presence of the complex solid solutions as discussed in section (c). S content varies between the spheres although a high content may suggest some surface enrichment commonly undergone by aerosols such as K_2SO_4[8]. Also present in the spheres is Fe, which has been shown to be catalytically important for their formation[24].

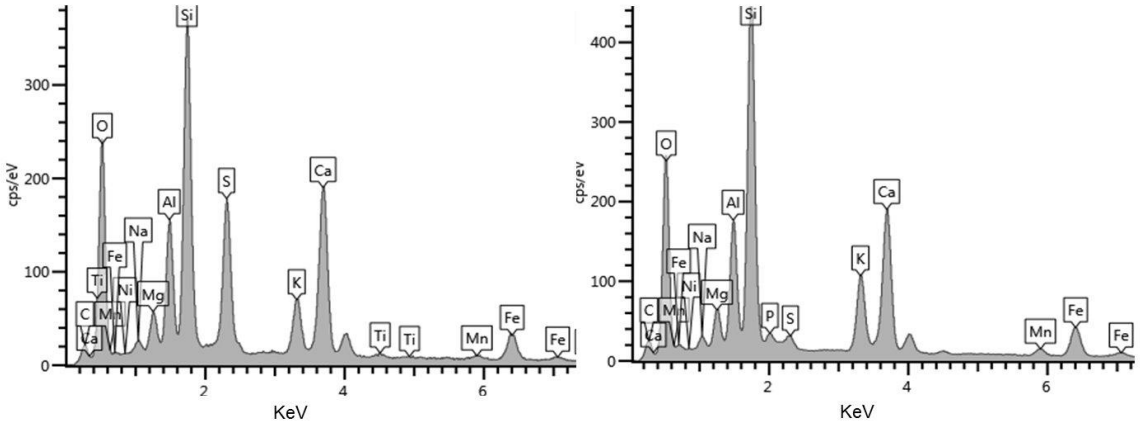

Figure 11: EDS spectrum of spheres in Figure 10e.

7. Conclusions

An investigation of fly ash deposition and loose oxide structure from a combustion run of co-fired eucalyptus and Russian coal under different temperatures and atmospheres has been conducted. Metal oxide scales have been observed in the loose deposits from the 15Mo3 probes and are visible under both reducing and oxidising conditions. Variation between the composition of these scales was found, this is thought to be due to the higher occurrence of KCl under a reducing atmosphere which in turn leads to greater rates of breakaway oxidation around the grain boundaries.

Under oxidising conditions whiskers, which are thought to be hematite, have been observed, further work to establish their composition using FIB-TEM is required. Magnetite crystals with an octahedral morphology are present under all conditions, indicating that in part the 15Mo3 alloy may have undergone active oxidation in order for the oxide scales to become loose.

The variation of spherical debris present indicates complex reactions occurring both pre and post deposition. Further analysis is required to allow identification of these spheres as either plerospheres or cenospheres.

8. Acknowledgements

The Authors would like to express thanks to the E.On New Build and Technology Centre, the Engineering and Physical Sciences Research Council (EPRSC), Materials Knowledge Transfer Network (Materials KTN) and Loughborough University for funding this work.

9. References

1. Kassman, H., Broström, M., Berg, M. & Åmand, L.-E. Measures to reduce chlorine in deposits: Application in a large-scale circulating fluidised bed boiler firing biomass. *Fuel* **90,** 1325–1334 (2011).

2. Furtado, H. & May, I. High temperature degradation in power plants and refineries. *Mater. Res.* **7,** 103–110 (2004).

3. Persson, K., Broström, M., Carlsson, J., Nordin, A. & Backman, R. High temperature corrosion in a 65 MW waste to energy plant. *Fuel Process. Technol.* **88,** 1178–1182 (2007).

4. Chang, Y.-N. Oxidation Behaviors of Five Low-Alloy Structural Steels at 600°C. *Corros. Sci.* **50,** 3–10 (1994).

5. Chang, Y.-N. & Wei, F.-I. Review High temperature oxidation of low alloy steels. *J. Mater. Sci.* **24,** 14–22 (1989).

6. Higginson, R. L., Jepson, M. a. E. & West, G. D. Use of EBSD to characterise high temperature oxides formed on low alloy and stainless steels. *Mater. Sci. Technol.* **22,** 1325–1332 (2006).

7. Skrifvars, B.-J., Backman, R., Hupa, M., Salmenoja, K. & Vakkilainen, E. Corrosion of superheater steel materials under alkali salt deposits Part 1: The effect of salt deposit composition and temperature. *Corros. Sci.* **50,** 1274–1282 (2008).

8. Loo, S. Van & Koppejan, J. *The handbook of biomass combustion and co-firing*. (Earthscan, 2008).

9. Zbogar, A., Frandsen, F., Jensen, P. A. & Glarborg, P. Shedding of ash deposits. *Prog. Energy Combust. Sci.* **35,** 31–56 (2009).

10. Jenkins, B., Baxter, L., Jr, T. M. & Miles, T. Combustion properties of biomass. *Fuel Process. Technol.* **54,** 17–46 (1998).

11. Vassilev, S. V., Baxter, D., Andersen, L. K. & Vassileva, C. G. An overview of the composition and application of biomass ash. Part 1. Phase–mineral and chemical composition and classification. *Fuel* **105,** 40–76 (2013).

12. Jappe Frandsen, F. Utilizing biomass and waste for power production—a decade of contributing to the understanding, interpretation and analysis of deposits and corrosion products. *Fuel* **84,** 1277–1294 (2005).

13. Kassman, H., Bäfver, L., Åmand, L., Power, V. & Ab, C. Sulphation of Gaseous KCl in a Biomass Fired CFB Boiler. in *Eur. Combust. Meet.* **3,** 2–7 (2009).

14. Uusitalo, M. ., Vuoristo, P. M. . & Mäntylä, T. . High temperature corrosion of coatings and boiler steels below chlorine-containing salt deposits. *Corros. Sci.* **46,** 1311–1331 (2004).

15. Nielsen, H. P., Frandsen, F. J., Dam-Johansen, K. & Baxter, L. L. The implications of chlorine-associated corrosion on the operation of biomass-fired boilers. *Prog. Energy Combust. Sci.* **26,** 283–298 (2000).

16. Gominho, J., Lourenço, A., Miranda, I. & Pereira, H. Chemical and fuel properties of stumps biomass from Eucalyptus globulus plantations. *Ind. Crops Prod.* **39,** 12–16 (2012).

17. D6349-09. *StandardTest Method for Determination of Major and Minor Elements in Coal , Coke , and Solid Residues from Combustion of Coal and Coke by Inductively Coupled Plasma — Atomic Emission*. **i,** 1–10 (ASTM, 2009).

18. Pettersson, C., Pettersson, J., Asteman, H., Svensson, J.-E. & Johansson, L.-G. KCl-induced high temperature corrosion of the austenitic Fe–Cr–Ni alloys 304L and Sanicro 28 at 600°C. *Corros. Sci.* **48,** 1368–1378 (2006).

19. Wood, G. C. I. Iron-Chromium Alloys and Stainless Steels at High Temperatures. *Corros. Sci.* **2,** 173–196 (1962).

20. Uusitalo, M. a., Vuoristo, P. M. J. & Mäntylä, T. a. Elevated temperature erosion–corrosion of thermal sprayed coatings in chlorine containing environments. *Wear* **252,** 586–594 (2002).

21. Park, S., Ji, W. & Kim, J. Effect of Chromium on the Corrosion Behaviour of Low-Alloy Steels Containing Copper in FGD Environment. *Int. J. Electrochem. Sci* **8,** 7498–7509 (2013).

22. Higginson, R. L. & Green, G. Whisker growth morphology of high temperature oxides grown on 304 stainless steel. *Corros. Sci.* **53,** 1690–1693 (2011).

23. Yuan, L. *et al.* The origin of hematite nanowire growth during the thermal oxidation of iron. *Mater. Sci. Eng. B* **177,** 327–336 (2012).

24. Raask, E. *Mineral Impurities in Coal Combustion: Behavior, Problems, and Remedial Measures*. 484 (Taylor & Francis, 1985).